

Article

A 12-Fold ThSi₂ Interpenetrated Network Utilizing a Glycine-Based Pseudopeptidic Ligand

Edward Loukopoulos , Alexandra Michail and George E. Kostakis * 

Department of Chemistry, School of Life Sciences, University of Sussex, Brighton BN1 9QJ, UK;

E.Loukopoulos@sussex.ac.uk (E.L.); alexandra_michail@hotmail.com (A.M.)

* Correspondence: G.Kostakis@sussex.ac.uk; Tel.: +44-1273-877-339

Received: 21 November 2017; Accepted: 15 January 2018; Published: 18 January 2018

Abstract: We report the synthesis and characterization of a 3D Cu(II) coordination polymer, [Cu₃(L¹)₂(H₂O)₈]·8H₂O (**1**), with the use of a glycine-based tripodal pseudopeptidic ligand (H₃L¹ = *N,N',N''*-tris(carboxymethyl)-1,3,5-benzenetricarboxamide or trimesoyl-tris-glycine). This compound presents the first example of a 12-fold interpenetrated ThSi₂ (**ths**) net. We attempt to justify the unique topology of **1** through a systematic comparison of the synthetic parameters in all reported structures with H₃L¹ and similar tripodal pseudopeptidic ligands. We additionally explore the catalytic potential of **1** in the A³ coupling reaction for the synthesis of propargylamines. The compound acts as a very good heterogeneous catalyst with yields up to 99% and loadings as low as 3 mol %.

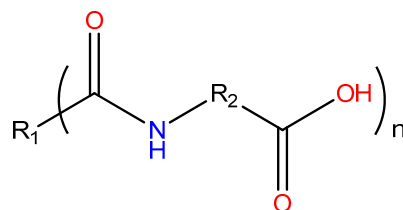
Keywords: coordination polymer; copper; interpenetration; 12-fold; catalysis; A³ coupling

1. Introduction

Ever since their popularization in the last decade, coordination polymers (CPs), also known as metal–organic frameworks (MOFs), have become one of the most prominent branches of inorganic and materials chemistry, in no small part due to the extensive variety of their applications [1–8]. A key factor for the rise of CPs as functional materials has been the development of rational synthetic routes towards the optimization of their application potential [9–12]. As a result, the strategic selection of a suitable ligand for the synthesis of CPs during the design of a new system is critical.

In recent years, a surge towards biologically derived CPs has been observed [13]. This type of compounds is typically constructed from bioligands such as amino acids, peptides, or nucleobases, which can offer a large variety for exploitation regarding possible coordination sites, the presence of functional groups, the degree of flexibility, and the potential formation of strong and weak interactions. This plethora of options has led to multiple reports of biologically related CPs with interesting applications: for example, porous CPs with adenine- [14], serine- [15], and dipeptide-based [16] ligands have been used successfully for the selective capture of CO₂. Furthermore, several ligands with amino acids or peptides have been employed with transition metals to induce chirality in various catalytic procedures [17–19]. Finally, CPs containing adenine have also been reported to have potential sensing [20] and drug storage [21] capabilities.

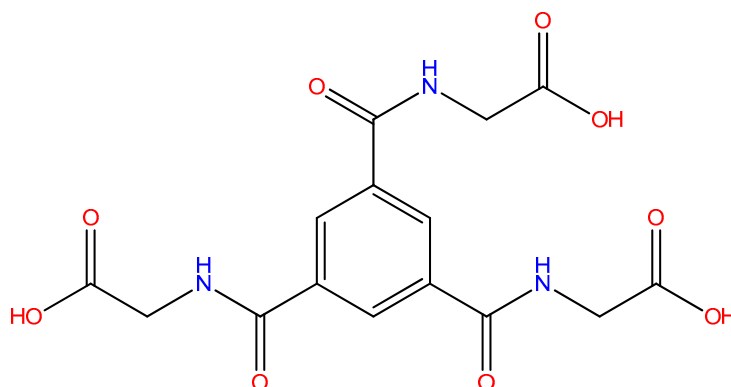
Pseudopeptidic ligands are another interesting type of biologically related linkers. In this case, a scaffold, which may be aromatic or nonaromatic, has amino acids or oligopeptides attached to it (Scheme 1). This type of ligands can offer multiple positions for coordination, as well as unlimited choices in flexibility, aromaticity, and hydrogen bond formation.



Scheme 1. General motif of pseudopeptidic ligands.

Our group [22–27] and others [28,29] have focused specifically on the coordination chemistry of pseudopeptidic ligands which retain a rigid aromatic scaffold, and introduced to it flexible amino acids. This strategy has produced a great variety of coordination polymers with many applications, such as luminescence [30], reversible water loss [27,30,31], magnetism [29], homochirality [18], and catalysis [26]. Additionally, this type of pseudopeptidic ligands are of great interest from a crystal engineering point of view and can lead to fascinating topologies due to: (a) the varying nature of the aromatic scaffold; (b) the possible formation of strong and weak hydrogen bonds as well as pi interactions; (c) the length of the amino acids; (d) the coordination abilities of the metal ion used.

Our most recent work in this project studied the influence of the Cu(II) salt on the resulting CPs when the pseudopeptidic ligand isophthaloylbis- β -alanine (H_2IBbA) was used [25]. Encouraged by the obtained result, we opted to investigate this effect on additional pseudopeptidic ligands. Having also in mind (a) our ongoing interest on CPs and their catalytic properties [32–34] and (b) the commonly limited solubility of these bulky pseudopeptidic CPs in organic solvents, we theorized that the resulting compounds could have an interesting activity as heterogeneous catalysts. Therefore, we herein present the synthesis, characterization, and topological evaluation of a novel compound formulated as $[Cu_3(L^1)_2(H_2O)_8] \cdot 8H_2O$ (**1**), where H_3L^1 is N,N',N'' -tris(carboxymethyl)-1,3,5-benzenetricarboxamide [35], also commonly known as trimesoyl-tris-glycine (Scheme 2). Furthermore, we report the catalytic activity of **1** in the metal-catalyzed multicomponent reaction (MCR) of an aldehyde, an amine, and an alkyne, also known as the A^3 coupling, towards the synthesis of propargylamines.



Scheme 2. The organic ligand H_3L^1 used in this study.

2. Experimental Section

2.1. Materials

Chemicals (reagent grade) were purchased from Sigma Aldrich (Gillingham, UK), Acros Organics (Loughborough, UK), and Alfa Aesar (Lancashire, UK). All experiments were performed under aerobic conditions using materials and solvents as received. Ligand H_3L^1 was synthesized according to the reported procedure [23].

2.2. Instrumentation

IR spectra of the samples were recorded over the range of 4000–650 cm^{-1} on a Perkin Elmer Spectrum One FT-IR spectrometer (Seer Green, UK) fitted with a UATR polarization accessory. EI-MS was performed on a VG Autospec Fissions instrument (EI at 70 eV, SIS, Ringoes, NJ, USA). TGA analysis was performed on a TA Instruments Q-50 model (TA, Surrey, UK) under nitrogen and at a scan rate of 10 $^{\circ}\text{C}/\text{min}$. NMR spectra were measured on a Varian VNMRS solution-state spectrometer (Agilent, Stockport, UK) at 30 $^{\circ}\text{C}$. Chemical shifts were quoted in parts per million (ppm). Coupling constants (J) were recorded in Hertz (Hz).

2.3. X-ray Crystallography

Data for compound **1** were collected (ω -scans) at the University of Sussex using an Agilent Xcalibur Eos Gemini Ultra diffractometer (Agilent, Stockport, UK) with a CCD plate detector (Agilent, Stockport, UK) under a flow of nitrogen gas at 173(2) K and Mo $\text{K}\alpha$ radiation ($\lambda = 0.71073 \text{ \AA}$). CRYCALIS CCD and RED software (version 1.171.38.41) were used, respectively, for data collection and processing. Reflection intensities were corrected for absorption by the multiscan method. The structure was determined using Olex2 [36], solved using SHELXT (version 2015) [37,38], and refined with SHELXL-2014 [39]. All non-H atoms were refined with anisotropic thermal parameters, and H-atoms were introduced at calculated positions and allowed to ride on their carrier atoms. For certain water lattice molecules, the introduction of H atoms at calculated positions led to an unsatisfactory structure solution with certain short intramolecular D–H \cdots H–D distances. Because of the poor quality of the crystallographic data in three different datasets, we were unable to locate these H atoms manually. For this reason, bond distances and angles regarding these atoms were not mentioned further. Additional measurements of elemental and TGA analysis were performed to conclusively validate the suggested formula and structure. Crystal data and structure refinement parameters for **1** are given in Table S1. The geometric and crystallographic calculations were performed using PLATON (version 1.18) [40], Olex2 (version 1.2) [36], and WINGX [41] packages (version 2014.1). The graphics were prepared with Crystal Maker and MERCURY [42], CCDC 1586912.

2.4. Synthetic Procedures

2.4.1. Synthesis of $[\text{Cu}_3(\text{L}^1)_2(\text{H}_2\text{O})_8]\cdot 8\text{H}_2\text{O}$ (**1**)

Method 1: 0.5 mmol (0.190 g) of H_3L^1 and 0.75 mmol (110 μL) of Et_3N were dissolved in 15 mL of H_2O while stirring to produce a colourless solution. To this, 1 mmol (0.232 g) of $\text{Cu}(\text{NO}_3)_2\cdot 2.5\text{H}_2\text{O}$ was added. The resulting light blue solution was stirred for a further 20 min at room temperature. After the end of the reaction, the solution was filtrated and then carefully layered over Me_2CO at a respective ratio of 1:2. After 6 days, large blue block crystals of **1**, as well as colourless needles of H_3L^1 were formed. Yield: 27% (based on Cu). *Method 2:* the same procedure as above was followed, but a solution of $\text{H}_2\text{O}/\text{MeOH}$ (10:1) was used instead of H_2O to produce only crystals of **1**. Yield: 18% (based on Cu). Selected IR peaks (cm^{-1}): 3253 (br), 1626 (m), 1557 (m), 1499 (w), 1434 (m), 1403 (m), 1304 (w), 1003 (w), 909 (w), 733 (m). Elemental analysis for $\text{C}_{30}\text{H}_{62}\text{Cu}_3\text{N}_6\text{O}_{34}$: calcd. C 43.89, H 5.04, N 6.78; found C 43.84, H 5.06, N 6.89.

2.4.2. General Catalytic Protocol for A^3 Coupling

A mixture of aldehyde (0.5 mmol), amine (0.55 mmol), alkyne (0.6 mmol), Cu catalyst **1** (3 mol%, based on aldehyde amount), and 2-propanol (2 ml) was added into a sealed tube and stirred at 90 $^{\circ}\text{C}$ for 12 h. After completion of the reaction, the mixture was allowed to cool down. The slurry was then filtered to withhold the catalyst, and the filtrate was evaporated under vacuum. The yield of the propargylamine products were then determined by their $^1\text{HNMR}$ spectra, which were compared with the data reported in the corresponding literature [34].

3. Results

3.1. Crystal Structure Description

Compound **1** crystallizes in the noncentrosymmetrical monoclinic Pn space group. X-ray determination of the crystal structure reveals the formation of an interpenetrated neutral three-dimensional coordination polymer (Figures 1 and 2). The asymmetric unit of **1** consists of 3 copper centres, 2 fully deprotonated ligand (L^1)³⁻ molecules, and a total of 16 water molecules; out of these, 8 act as terminal ligands and 8 are present in the lattice. In both (L^1)³⁻ molecules, each of the three carboxylate groups coordinate to each of the three Cu centers. Additionally, in both ligands, the three amido groups exist in a *trans* conformation and all of them are in *anti* conformation (Figure 3). Cu1 is coordinated to six atoms and exhibits a distorted octahedral geometry ($s/h = 1.04$, $\phi = 52.9^\circ$ [43]). The equatorial positions of this octahedron are occupied by four carboxylate oxygen atoms deriving from two different ligands. Cu2 and Cu3 are each coordinated to five atoms and exhibit a square pyramidal geometry ($\tau = 0.06$ for Cu2, 0.17 for Cu3 [44]). In the coordination environment of both metal centers, the basal plane consists of two oxygen atoms from two different ligand molecules, as well as two oxygen atoms from terminal water molecules. An oxygen atom from another terminal water molecule occupies the apical position in both cases. Selected bond lengths are listed in Table 1. The Cu–Cu distances between the metal centers range from 11.400(3) to 14.176(3) Å. Furthermore, the crystal structure of **1** is stabilized by strong intermolecular O–H···O hydrogen bonds, which involve the oxygen atoms of all 16 water molecules as donors. The atoms involved as acceptors in these bonds are oxygen atoms of either water molecules or the carbonyl group of the amide.

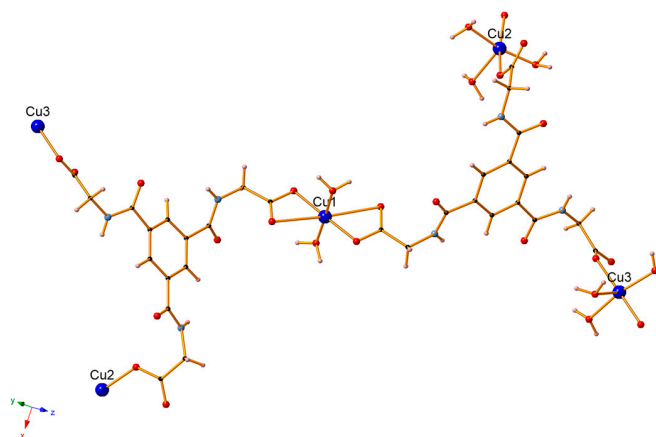


Figure 1. The crystal structure of **1**. Lattice water molecules are omitted for clarity. Colour code: Cu (blue), C (black), H (light pink), N (light blue), O (red).

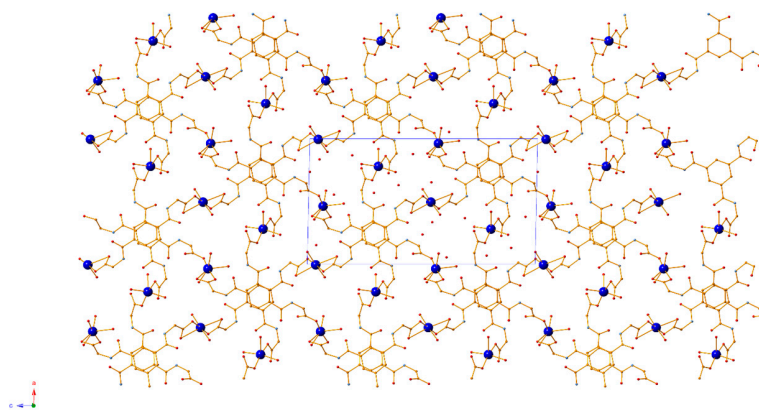


Figure 2. Packing diagram for **1** along the $a0c$ plane.

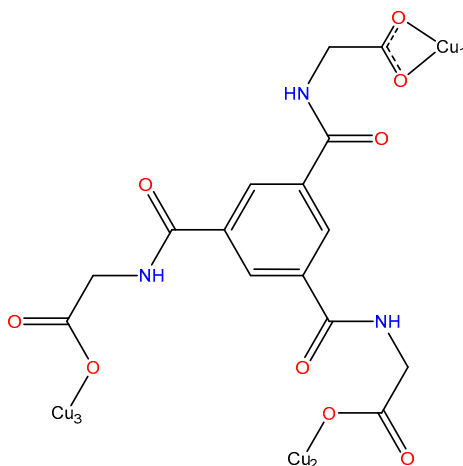


Figure 3. Coordination mode of the $(L^1)^{3-}$ organic ligand found in **1**.

Table 1. Selected bond lengths (Å) for **1**.

Bond	Å
Cu1–O1	1.932(11)
Cu1–O2	2.668(11)
Cu1–O10	1.964(10)
Cu1–O11	2.611(11)
Cu1–O19	1.938(11)
Cu1–O20	1.931(10)
Cu2–O8	1.942(11)
Cu2–O28	1.991(9)
Cu2–O29	2.191(11)
Cu2–O30	1.959(10)
Cu2–O14 ¹	1.927(11)
Cu3–O5	1.928(10)
Cu3–O22	1.925(12)
Cu3–O23	2.005(11)
Cu3–O24	2.343(11)
Cu3–O18 ²	1.943(10)
Cu1–Cu2	11.400(3)
Cu1–Cu3	14.176(3)
Cu2–Cu3	12.554(3)

Symmetry Operators: ¹ $-3/2 + X, 2 - Y, 1/2 + Z$; ² $+X, -2 + Y, 1 + Z$.

3.2. Topological Analysis

The complicated structure of compound **1** can be simplified into a net considering each ligand as a three-connected node and each metal center as a two-connected node; therefore, the two-connected nodes are not further considered for the classification. The final outcome of the topological analysis of the three-dimensional coordination polymer **1**, with the use of the TOPOS software [45] and the standard representation methodology, is a three-connected, 12-fold interpenetrated symmetric **ths** net (Figure 4). According to a literature survey in the TOPOS and CCDC databases, compounds EJISAS [46] and KOBFEN [47] can be also represented as 12-fold **ths** nets; however, this simplification derives when a standard representation is selected. The topological analysis of the latter two compounds using the standard cluster representation and considering the $\text{Cu}(\text{O}_2)\text{Cu}$ as nodes [48], yields a 12-fold interpenetrated diamond (**dia**) net, therefore compound **1** represents the first example of a standard 12-fold interpenetrated **ths** net.

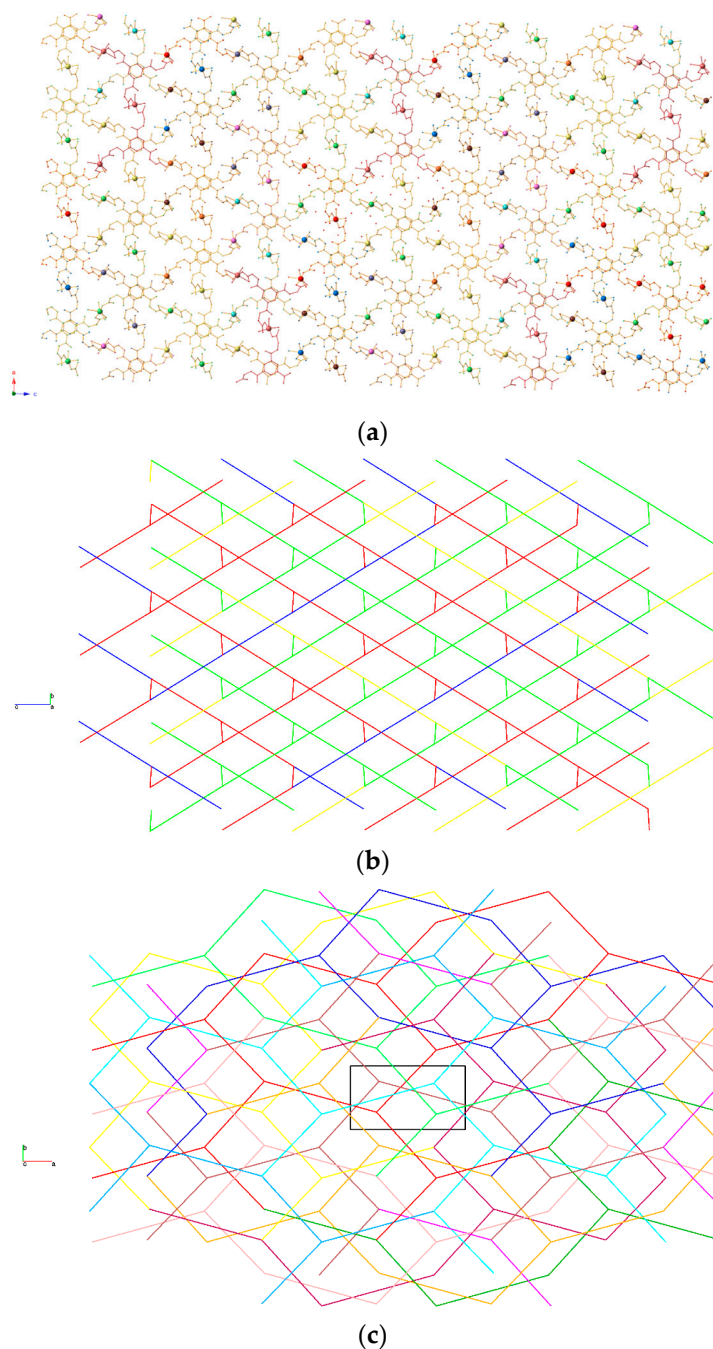


Figure 4. Simplified coloured versions of the 3D 12-fold interpenetrated ths network found in **1** along the $a0c$ (a), $b0c$ (b), $b0a$ (c) planes.

3.3. TGA and IR Studies

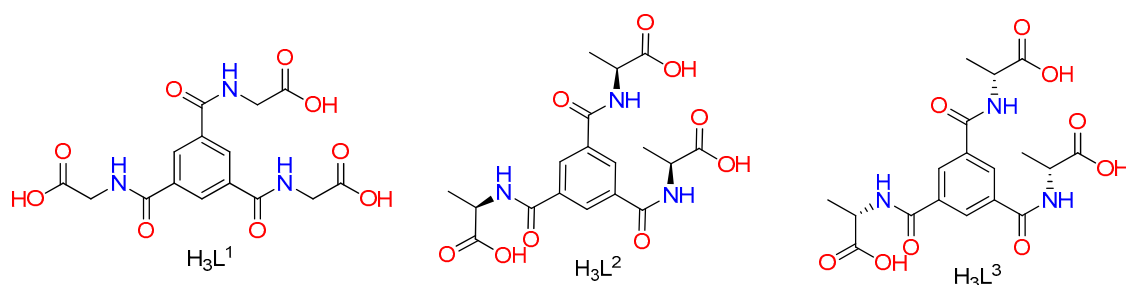
To examine the thermal behavior and stability of **1**, TGA was carried out between room temperature and 800 °C under N₂ atmosphere. This analysis (Figure S1) shows that the first mass loss is continuous, as it begins in the region of 50 °C and is completed at approximately 150 °C. This is attributed to the loss of eight lattice and eight ligated water molecules, in good agreement with the theoretical value (calc.: 23.60%, theor.: 23.25%). The remaining framework is then relatively stable up to ~310 °C, where it is subjected to a further mass loss due to decomposition to CuO (calc.: 63.14%, theor.: 65.14%). The reported peaks in the IR spectrum of **1** (Figure S2) are in good agreement with the crystallographic data. A broad absorption peak is found at 3253 cm⁻¹ and is attributed

to the stretching vibration of the O–H bonds. The peak at 1622 cm^{-1} is due to the presence of the noncoordinated carbonyl group of the amide, in good agreement with previously reported values for similar [23] compounds. Furthermore, peaks at 1557 and 1403 cm^{-1} can be attributed to the $\nu(\text{CO}_2)_{\text{as}}$ and symmetric $\nu(\text{CO}_2)_{\text{s}}$ bands of coordinated carboxylate groups, respectively. Finally, some peaks related possibly to C–H bending vibrations appear at 909 and 733 cm^{-1} .

3.4. Synthetic Aspects

Our initial efforts for the synthesis of **1** involved experiments in various ratios of water/alcohol media, based on our previous experiences with H_3L^1 [23] as well as the related literature [30]. However, no crystals were obtained in this case. The protocol was therefore modified with various techniques and ratios in order to facilitate crystallization. After extensive screening, liquid diffusion in acetone was found to be the only effective technique amongst the tested ones. The use of other suitable secondary crystallization solvents (e.g., acetonitrile) led, instead, to amorphous material. It is worth noting that the water/alcohol mix seems to be critical for the pure synthesis of **1**, as a similar experiment in H_2O also yielded crystals of the organic ligand; however, no MeOH molecules were found in the structure, despite their potential participation in H-bonding.

While the topology of **1** has not been observed before, the afforded compound is not the only structure which contains a Cu(II) source and the H_3L^1 ligand. In fact, a search in the CCDC [49] revealed a variety of structures, but all of these show a different topology. To shed more light into this as well as attempt to rationalize the synthesis, we opted to perform a more systematic search in the literature for similar tripodal pseudopeptidic ligands. This narrowed our results to a total of 28 reported coordination compounds, with 3 different ligands depending on the varying amino acid: either Glycine (H_3L^1), L-Alanine (H_3L^2), or D-Alanine (H_3L^3) (Scheme 3). To provide a full insight, we included a full list of factors that could point towards the resulting differences. These parameters included the metal ion, the synthetic conditions including solvent and temperature, and the presence of a base or a second organic linker. These are listed in detail in Table 2.



Scheme 3. The tripodal pseudopeptidic ligands compared in this study.

In regard to the H_3L^1 glycine-based ligand, a comparison between our result (Entry 1) and the rest of the reported Cu(II) compounds (entries 2–5) already revealed major influences of these parameters. Compound **1** was synthesized using $\text{Cu}(\text{NO}_3)_2 \cdot 2.5\text{H}_2\text{O}$, while, in the rest of the relevant entries, $\text{CuCl}_2 \cdot 2\text{H}_2\text{O}$ was used as the metal source. The role of the metal ion in the resulting structure has already been reported, especially for Cu(II) sources in similar pseudopeptidic ligands. Therefore, our result further confirmed this effect. The rest of the parameters revealed additional interesting information: a comparison of entries 2–4 showed that the presence and amount of base (and as a consequence, the tuning of pH) led to different structures; in the case of entry 4, the base (pyridine) actually coordinated to the metal center, which led to a 2D coordination polymer instead of a 3D, and to a less exciting topology. Regarding the synthetic conditions between these entries, a possible temperature effect over time could be observed. Efforts to obtain a crystal structure using $\text{CuCl}_2 \cdot 2\text{H}_2\text{O}$ and the synthetic method of **1**, or $\text{Cu}(\text{NO}_3)_2 \cdot 2.5\text{H}_2\text{O}$ and solvothermal conditions were unfortunately unsuccessful. However, we could obtain a wider scope for conclusions by bringing

also the glycine-based compounds with other metals (entries 6–20) into the comparison. Through this, it is worth noting the following: (a) the compounds of entries 2 and 6–9 had a general formula of $[M(L^1)(H_2O)_3]_2[M(H_2O)_6] \cdot (H_2O)_3$ regardless of the synthetic method; (b) our attempts to utilize our synthetic method with other metals (Co, Zn, Mn) resulted in the same crystal structures in entries 2 and 6–9, conclusively proving that the synthetic procedures were not the prevalent factor in order to get structures with the 12-fold topology; (c) as expected, the presence of a second organic linker led to even more unpredictable structures. Interestingly, a comparison between entries 5 and 12 (Cu- and Co-based respectively), in which the same linker (bpp) and similar synthetic methods were employed, revealed significant differences in the resulting products, further pointing to the lesser importance of the conditions compared to the choice of metal; (d) a comparison between Ca(II)-based compounds $[Ca_6(L^1)_4(H_2O)_{14}](H_2O)_3$ and $[Ca_2(HL^1)_2(\mu-H_2O)(H_2O)_5] \cdot 3H_2O$ (entries 18 and 19 respectively), which were synthesized under very similar methods but with a different Ca(II) source (chloride for entry 18, nitrate for 19), further pointed towards the metal ion influence; (e) only the metals with flexibility in their coordination environment and geometry (copper, alkaline earth metals, lanthanides) provided any cases of structural variety. Interestingly, the largest variety of compounds was observed when Cu(II) sources were employed.

Table 2. Overview of the synthetic parameters and topology of all reported compounds with tripodal pseudopeptidic ligands.

Entry	Metal Salt	L	Additive ^a	Conditions	Formula	Ref.
1	Cu(NO ₃) ₂ ·2.5H ₂ O	H ₃ L ¹	Et ₃ N	rt/H ₂ O/MeOH (10:1)/Me ₂ CO	[Cu ₃ (L ¹) ₂ (H ₂ O) ₈]·8H ₂ O	^b
2	CuCl ₂ ·2H ₂ O	H ₃ L ¹	None	100 °C/3 h/H ₂ O/DMF (1:2)	[Cu(L ¹)(H ₂ O) ₃] ₂ [Cu(H ₂ O) ₆]·(H ₂ O) ₃	[50]
3	CuCl ₂ ·2H ₂ O	H ₃ L ¹	py ^c	100 °C/24 h/H ₂ O/DMF (1:1)	[Cu ₃ (L ¹) ₂ (H ₂ O) ₃]·2H ₂ O	[50]
4	CuCl ₂ ·2H ₂ O	H ₃ L ¹	py	90 °C/40 h/H ₂ O/DMF (1:1)	[Cu ₂ (L ¹)(Py) ₂ (μ ₃ -OH)]·(H ₂ O) ₂	[50]
5	CuCl ₂ ·2H ₂ O	H ₃ L ¹	bpp ^d	100 °C/48 h/H ₂ O/MeOH (1:1)	[Cu ₂ (L ¹)(bpp)(μ ₃ -OH)]·6H ₂ O	[50]
6	Zn(NO ₃) ₂ ·2.5H ₂ O	H ₃ L ¹	None	100 °C/48 h/H ₂ O/MeOH (10:1)	[Zn(L ¹)(H ₂ O) ₃] ₂ [Zn(H ₂ O) ₆]·(H ₂ O) ₃	[30]
7	Ni(NO ₃) ₂ ·2.5H ₂ O	H ₃ L ¹	None	100 °C/48 h/H ₂ O/MeOH (10:1)	[Ni(L ¹)(H ₂ O) ₃] ₂ [Ni(H ₂ O) ₆]·(H ₂ O) ₃	[30]
8	Mn(OAc) ₂ ·4H ₂ O	H ₃ L ¹	None	100 °C/48 h/H ₂ O/MeOH (10:1)	[Mn(L ¹)(H ₂ O) ₃] ₂ [Mn(H ₂ O) ₆]·(H ₂ O) ₃	[30]
9	Co(NO ₃) ₂ ·6H ₂ O	H ₃ L ¹	None	100 °C/48 h/H ₂ O/MeOH (10:1)	[Co(L ¹)(H ₂ O) ₃] ₂ [Co(H ₂ O) ₆]·(H ₂ O) ₃	[30]
10	Co(NO ₃) ₂ ·6H ₂ O	H ₃ L ¹	bpy ^e	100 °C/48 h/H ₂ O	[Co _{1.5} (L ¹)(bpy) _{1.5} (H ₂ O) ₃]·(H ₂ O) ₅	[51]
11	Co(NO ₃) ₂ ·6H ₂ O	H ₃ L ¹	bpe ^f	100 °C/48 h/H ₂ O	[Co _{1.5} (L ¹)(bpe) _{1.5} (H ₂ O) ₂]	[51]
12	Co(NO ₃) ₂ ·6H ₂ O	H ₃ L ¹	bpp	100 °C/48 h/H ₂ O	[Co ₂ (L ¹)(bpp) ₂ (NO ₃)(μ ₂ -H ₂ O) ₂]·(H ₂ O) ₂	[51]
13	Tb(III)	H ₃ L ¹	None	N/A ^g	[Tb(L ¹)(H ₂ O) ₃]·H ₂ O	[31]
14	Gd(III)	H ₃ L ¹	None	N/A	[Gd(L ¹)(H ₂ O) ₃]·H ₂ O	[31]
15	Nd(III)	H ₃ L ¹	None	N/A	[Nd(L ¹)(H ₂ O) ₃]·H ₂ O	[31]
16	La(III)	H ₃ L ¹	None	N/A	[La(L ¹)(EtOH)(H ₂ O) ₂]·2.5H ₂ O	[31]
17	CaCl ₂	H ₃ L ¹	py	rt/H ₂ O/MeOH (1:1)	[Ca(HL ¹)(H ₂ O) ₂]	[52]
18	CaCl ₂	H ₃ L ¹	py	rt/H ₂ O/MeOH (1:1)	[Ca ₆ (L ¹) ₄ (H ₂ O) ₁₄](H ₂ O) ₃	[52]
19	Ca(NO ₃) ₂ ·3H ₂ O	H ₃ L ¹	NaOAc	rt/H ₂ O/EtOH (1:1)	[Ca ₂ (HL ¹) ₂ (μ-H ₂ O)(H ₂ O) ₅]·3H ₂ O	[23]
20	Sr(NO ₃) ₂	H ₃ L ¹	NaOAc	rt/H ₂ O/EtOH (1:1)	[Sr ₂ (HL ¹) ₂ (H ₂ O) ₇]·H ₂ O	[23]
21	Cu(NO ₃) ₂ ·3H ₂ O	H ₃ L ²	KOH/am ^h	80 °C/48 h/MeOH/DMF (10:1)	[Cu ₄ (HL ²) ₂ (H ₂ O) ₄ (MeO) ₄]	[53]
22	CuCl ₂ ·2H ₂ O	H ₃ L ²	KOH	rt/EtOH/DMF (4:1)	[Cu ₁₂ (L ²) ₈ (H ₂ O) ₁₂]·8EtOH·40H ₂ O	[54]
23	Zn(NO ₃) ₂ ·6H ₂ O	H ₃ L ²	bpy/KOH	rt/H ₂ O/MeOH (3:8)	[Zn ₃ (L ²) ₂ (bpy) ₄]·24H ₂ O	[55]
24	Ni(NO ₃) ₂ ·2H ₂ O	H ₃ L ²	bpy/KOH	95 °C/48 h/H ₂ O/EtOH (1:1)	[Ni ₃ (L ²) ₂ (bpy) ₄]·2EtOH·14H ₂ O	[56]
25	Co(NO ₃) ₂ ·2H ₂ O	H ₃ L ²	bpy/KOH	rt/H ₂ O/MeOH (3:8)	[Co ₃ (L ²) ₂ (bpy) ₄]·28H ₂ O	[56]
26	Cd(NO ₃) ₂ ·4H ₂ O	H ₃ L ²	bpy/teda ⁱ	100 °C/72 h/H ₂ O/DMF (1:1)	[Cd ₈ (L ²) ₆ (bpy) ₃ (H ₂ O) ₄](H ₃ O) ₂	[18]
27	Ni(NO ₃) ₂ ·2H ₂ O	H ₃ L ³	bpy/KOH	95 °C/48 h/H ₂ O/EtOH (1:1)	[Ni ₃ (L ³) ₂ (bpy) ₄]·2EtOH·14H ₂ O	[56]
28	Co(NO ₃) ₂ ·2H ₂ O	H ₃ L ³	bpy/KOH	rt/H ₂ O/MeOH (3:8)	[Co ₃ (L ³) ₂ (bpy) ₄]·28H ₂ O	[56]
29	Cd(NO ₃) ₂ ·4H ₂ O	H ₃ L ³	bpy/teda	100 °C/72 h/H ₂ O/DMF (1:1)	[Cd ₈ (L ³) ₆ (bpy) ₃ (H ₂ O) ₄](H ₃ O) ₂	[18]

^a Refers to the use of any base or secondary organic linker. ^b This work. ^c py = pyridine. ^d bpp = (1,3-di(4-pyridyl)propane).

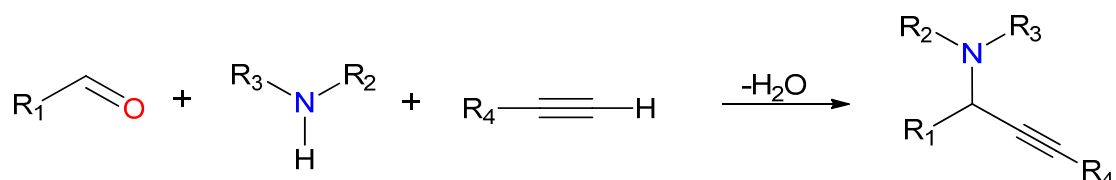
^e bpy = 4,4'-bipyridine. ^f bpe = [1,2-bi(4-pyridyl)ethane]. ^g N/A = Not available. ^h am = ammonium hydroxide,

ⁱ teda = Triethylenediamine.

In regard to the alanine-based compounds (entries 21–29), the presence of an additional methyl group led to completely different compounds and topologies, as expected. However, the stark difference in entries 21 and 22 (in which Cu(NO₃)₂·3H₂O and CuCl₂·2H₂O were employed respectively) once again strongly suggests a metal ion influence towards the resulting product. In summary, when exploring the coordination chemistry of this type of pseudopeptidic ligands, the choice of the metal ion seems to play an important role towards the resulting product and, as a consequence, in the resulting topology and interpenetration.

3.5. Catalytic Studies

The A^3 coupling (Scheme 4) has been widely studied in recent years [57–61], as the resulting propargylamines have been proposed as key intermediates in the synthesis of various N-containing biologically active compounds [62–65]. Even though many metal sources and compounds, including CPs [66–69], have been tested as catalysts for this reaction, Cu(II) CPs have been used very rarely [34].



Scheme 4. General overview of the multicomponent reaction of aldehydes, amines, and alkynes (A^3 coupling).

In order to test the possible catalytic activity of **1**, initial studies were performed for the A^3 coupling of cyclohexane carboxaldehyde, pyrrolidine, and phenylacetylene. After extensive screening, optimal conditions were obtained when the mixture was stirred for 24 h in the presence of 2-propanol (iPrOH) [70], at 90 °C, under air atmosphere, and by adding only 0.03 mmol of compound **1** (in 1 mmol reaction scale of aldehyde). To our delight, these conditions accounted for quantitative yields of the model propargylamine; this accumulated to a turnover number of 33.3 for the catalyst. Additionally, no reaction was observed in the absence of **1**, result that further supports the activity of the catalyst in the studied multicomponent coupling.

We then employed a variety of aldehydes, amines, and alkynes as substrates in order to study the scope of the reaction. Amine screening, as presented in Table 3, entries 1–6, indicated that cyclic secondary amines afford the corresponding propargylamine products in excellent yields, while acyclic secondary amines were found to be slightly less effective. Results of the aldehyde screening (entries 7–10) revealed that aromatic aldehydes show slightly lower reactivity. Furthermore, the reactivity and respective yields were affected by the presence of an electron-donating or electron-withdrawing group in the aldehyde. In comparison, saturated aliphatic aldehydes displayed high reactivity and afforded excellent yields. In regard to the alkyne selection, the employment of either phenylacetylene or 1-hexyne resulted to the corresponding propargylamines in excellent yields when the model aldehyde and amine substrates were also used. The relevant results can be found as entries 1 and 11.

Table 3. Catalytic activity of **1** in the A^3 coupling.

Entry	Aldehyde	Amine	Alkyne	Yield ^a (%)
1	cyclohexane carboxaldehyde	pyrrolidine	phenylacetylene	99
2	cyclohexane carboxaldehyde	piperidine	phenylacetylene	99
3	cyclohexane carboxaldehyde	azepane	phenylacetylene	94
4	cyclohexane carboxaldehyde	morpholine	phenylacetylene	99
5	cyclohexane carboxaldehyde	diethylamine	phenylacetylene	77
6	cyclohexane carboxaldehyde	<i>N</i> -methylaniline	phenylacetylene	58
7	benzaldehyde	pyrrolidine	phenylacetylene	67
8	4-methyl benzaldehyde	pyrrolidine	phenylacetylene	61
9	4-methoxy benzaldehyde	pyrrolidine	phenylacetylene	36
10	4-chloro benzaldehyde	pyrrolidine	phenylacetylene	64
11	cyclohexane carboxaldehyde	pyrrolidine	1-hexyne	95
12	cyclohexane carboxaldehyde	pyrrolidine	phenylacetylene	96 ^b

^a NMR yields based on aldehyde. ^b After the fourth cycle of catalyst use.

The characterization by TGA and IR spectroscopy pointed towards a similar identity of this solid compared to bulk samples of **1** (Figures S3 and S4). The compound showed no solubility in common organic solvents during our tests; therefore, the next step was to study the heterogeneous nature and capabilities of the recycled compound. The catalyst could be easily recovered by filtration after the end of the reactions and then be reused after treatment with acetone and diethyl ether to remove any reagents or product. The simulated and the “as is” synthesized compound powder XRD patterns were in good agreement, however the spectrum of the postcatalysis recovered solid (Figure S5) appeared to be similar to the XRD pattern of the reported compounds with the general formula $[M(L^1)(H_2O)_3]_2[M(H_2O)_6] \cdot (H_2O)_3$ (Table 2, entry 2; CCDC entry SIDJIZ was selected for comparison). This indicates that a phase transition or structure change of compound **1** to the corresponding SIDJIZ probably took place during the catalytic procedure. This phenomenon could not to be detected by TGA and IR measurements because of the similarities in the general formula. Experiments carried out with the model reaction and the recovered material showed that it can be reused at least four times with only a slight decrease in the catalytic activity (Table 3, entry 12). Because of the lack of porous channels within the structure of **1**, as well as the similar performance of the transformed recovered material, we envisage that the observed catalytic activity was revealed on the surface of the coordination polymer.

4. Conclusions

To summarize, in this work, we have continued our studies on the coordination chemistry of pseudopeptidic ligands. We synthesized a new three-dimensional Cu(II) coordination polymer with the tripodal trimesoyl-tris-glycine ligand. Compound **1** has a unique topological standard representation and can be considered as the first example of a 12-fold interpenetrated **ths** network. Synthetic-wise, a systematic study and comparison of all reported structures with this ligand and similar tripodal pseudopeptidic ligands showed that the choice of the Cu(II) starting material can have a large influence towards the self-assembly of the resulting product. Furthermore, **1** showed good catalytic activity towards the multicomponent synthesis of propargylamines under mild conditions; it was anticipated that the catalysis took place on the surface of the coordination polymer because of the lack of porosity. The recovered material could be reused for at least four cycles, however, PXRD studies pointed towards a structural change to a more favourable framework during the catalytic procedure. As such, the catalytic activity of **1** does not appear extremely promising for further efforts. Nevertheless, these initial results certainly demonstrate that coordination compounds with pseudopeptidic ligands could be tested as potential catalysts in organic reactions, provided that their structural framework remains stable. As a result of the above, our future efforts will thus focus on: (a) employing a variety of Cu(II) sources in more pseudopeptidic ligands to further study the self-assembly effect; (b) attempting to exploit the effect in order to get more interesting topologies; (c) identifying similar pseudopeptidic coordination compounds with higher stability in order to study their catalytic potential.

Supplementary Materials: The following are available online at www.mdpi.com/2073-4352/8/1/47/s1, Table S1: Crystal data and structure refinement for **1**; Figure S1: TGA graph for compound **1**, Figure S2: The IR spectrum of compound **1**, Figure S3: TGA graph for the recycled catalyst, Figure S4: TGA overlay of **1** (green) and the recycled catalyst (red), Figure S5: PXRD overlay of **1** pre- (red) and post- (black) catalysis. The simulated pattern of refile SIDJIZ (mauve) is included for comparison; 1H NMR of product propargylamines.

Acknowledgments: Vladislav Blatov and Davide Proserpio are acknowledged for helpful scientific discussions. Smaragda Lymperopoulou (University of Southampton, UK) is acknowledged for recording the PXRD data.

Author Contributions: Edward Loukopoulos and George E. Kostakis conceived and designed the experiments; Edward Loukopoulos and Alexandra Michail performed the experiments; Edward Loukopoulos, Alexandra Michail, and George E. Kostakis analysed the data; Edward Loukopoulos and George E. Kostakis wrote the paper.

Conflicts of Interest: The authors declare no conflict of interest.

References

1. Furukawa, H.; Cordova, K.E.; O’Keeffe, M.; Yaghi, O.M. The Chemistry and Applications of Metal-Organic Frameworks. *Science* **2013**, *341*, 1230444. [[CrossRef](#)] [[PubMed](#)]
2. Li, B.; Wen, H.M.; Cui, Y.; Zhou, W.; Qian, G.; Chen, B. Emerging Multifunctional Metal–Organic Framework Materials. *Adv. Mater.* **2016**, *28*, 8819–8860. [[CrossRef](#)] [[PubMed](#)]
3. Zhu, L.; Liu, X.Q.; Jiang, H.L.; Sun, L.B. Metal-Organic Frameworks for Heterogeneous Basic Catalysis. *Chem. Rev.* **2017**, *117*, 8129–8176. [[CrossRef](#)] [[PubMed](#)]
4. Yu, J.; Xie, L.-H.; Li, J.-R.; Ma, Y.; Seminario, J.M.; Balbuena, P.B. CO₂ Capture and Separations Using MOFs: Computational and Experimental Studies. *Chem. Rev.* **2017**, *117*, 9674–9754. [[CrossRef](#)] [[PubMed](#)]
5. Kirillov, A.M.; Karabach, Y.Y.; Kirillova, M.V.; Haukka, M.; Pombeiro, A.J.L. Topologically unique 2D heterometallic Cu II/Mg coordination polymer: Synthesis, structural features, and catalytic use in alkane hydrocarboxylation. *Cryst. Growth Des.* **2012**, *12*, 1069–1074. [[CrossRef](#)]
6. Liu, B. Metal–organic framework-based devices: Separation and sensors. *J. Mater. Chem.* **2012**, *22*, 10094. [[CrossRef](#)]
7. Wu, M.X.; Yang, Y.W. Metal–Organic Framework (MOF)-Based Drug/Cargo Delivery and Cancer Therapy. *Adv. Mater.* **2017**, *29*, 1606134. [[CrossRef](#)] [[PubMed](#)]
8. Cui, Y.; Chen, B.; Qian, G. Lanthanide metal-organic frameworks for luminescent sensing and light-emitting applications. *Coord. Chem. Rev.* **2014**, *273–274*, 76–86. [[CrossRef](#)]
9. Zhang, M.; Bosch, M.; Gentle, T., III; Zhou, H.-C. Rational design of metal–organic frameworks with anticipated porosities and functionalities. *CrystEngComm* **2014**, *16*, 4069. [[CrossRef](#)]
10. Burneo, I.; Stylianou, K.; Imaz, I.; MasPOCH, D. The influence of the enantiomeric ratio of an organic ligand on the structure and chirality of Metal-Organic Frameworks. *Chem. Commun.* **2014**, *50*, 13829–13832. [[CrossRef](#)] [[PubMed](#)]
11. Loukopoulos, E.; Chilton, N.F.; Abdul-Sada, A.; Kostakis, G.E. Exploring the Coordination Capabilities of a Family of Flexible Benzotriazole-Based Ligands Using Cobalt(II) Sources. *Cryst. Growth Des.* **2017**, *17*, 2718–2729. [[CrossRef](#)]
12. Lu, W.; Wei, Z.; Gu, Z.-Y.; Liu, T.-F.; Park, J.; Park, J.; Tian, J.; Zhang, M.; Zhang, Q.; Gentle, T.; et al. Tuning the structure and function of metal-organic frameworks via linker design. *Chem. Soc. Rev.* **2014**, *43*, 5561–5593. [[CrossRef](#)] [[PubMed](#)]
13. Anderson, S.L.; Stylianou, K.C. Biologically derived metal organic frameworks. *Coord. Chem. Rev.* **2017**, *349*, 102–128. [[CrossRef](#)]
14. An, J.; Fiorella, R.P.; Geib, S.J.; Rosi, N.L. Synthesis, structure, assembly, and modulation of the CO₂ adsorption properties of a zinc-adeninate macrocycle. *J. Am. Chem. Soc.* **2009**, *131*, 8401–8403. [[CrossRef](#)] [[PubMed](#)]
15. Tan, Y.X.; He, Y.P.; Zhang, J. Serine-based homochiral nanoporous frameworks for selective CO₂ uptake. *Inorg. Chem.* **2011**, *50*, 11527–11531. [[CrossRef](#)] [[PubMed](#)]
16. Martí-Gastaldo, C.; Warren, J.E.; Stylianou, K.C.; Flack, N.L.O.; Rosseinsky, M.J. Enhanced stability in rigid peptide-based porous materials. *Angew. Chem. Int. Ed.* **2012**, *51*, 11044–11048. [[CrossRef](#)] [[PubMed](#)]
17. Wu, C.D.; Hu, A.; Zhang, L.; Lin, W. A homochiral porous metal-organic framework for highly enantioselective heterogeneous asymmetric catalysis. *J. Am. Chem. Soc.* **2005**, *127*, 8940–8941. [[CrossRef](#)] [[PubMed](#)]
18. Wu, X.; Zhang, H.-B.; Xu, Z.-X.; Zhang, J. Asymmetric induction in homochiral MOFs: From interweaving double helices to single helices. *Chem. Commun.* **2015**, *51*, 16331–16333. [[CrossRef](#)] [[PubMed](#)]
19. Wang, C.; Zheng, M.; Lin, W. Asymmetric catalysis with chiral porous metal-organic frameworks: Critical issues. *J. Phys. Chem. Lett.* **2011**, *2*, 1701–1709. [[CrossRef](#)]
20. An, J.; Shade, C.M.; Chengelis-Czegan, D.A.; Petoud, S.; Rosi, N.L. Zinc-adeninate metal-organic framework for aqueous encapsulation and sensitization of near-infrared and visible emitting lanthanide cations. *J. Am. Chem. Soc.* **2011**, *133*, 1220–1223. [[CrossRef](#)] [[PubMed](#)]
21. McKinlay, A.C.; Morris, R.E.; Horcajada, P.; Férey, G.; Gref, R.; Couvreur, P.; Serre, C. BioMOFs: Metal-organic frameworks for biological and medical applications. *Angew. Chem. Int. Ed.* **2010**, *49*, 6260–6266. [[CrossRef](#)] [[PubMed](#)]

22. Dokorou, V.N.; Milios, C.J.; Tsipis, A.C.; Hauka, M.; Weidler, P.G.; Powell, A.K.; Kostakis, G.E. Pseudopeptidic ligands: Exploring the self-assembly of isophthaloylbisglycine (H2IBG) and divalent metal ions. *Dalton Trans.* **2012**, *41*, 12501–12513. [[CrossRef](#)] [[PubMed](#)]
23. Dokorou, V.N.; Powell, A.K.; Kostakis, G.E. Two pseudopolymorphs derived from alkaline earth metals and the pseudopeptidic ligand trimesoyl-tris-glycine. *Polyhedron* **2013**, *52*, 538–544. [[CrossRef](#)]
24. Morrison, C.N.; Powell, A.K.; Kostakis, G.E. Influence of Metal Ion on Structural Motif in Coordination Polymers of the Pseudopeptidic Ligand Terephthaloyl-bis-beta-alaninate. *Cryst. Growth Des.* **2011**, *11*, 3653–3662. [[CrossRef](#)]
25. Lymperopoulou, S.; Dokorou, V.N.; Tsipis, A.C.; Weidler, P.G.; Plakatouras, J.C.; Powell, A.K.; Kostakis, G.E. Influence of the metal salt on the self-assembly of isophthaloylbis- β -alanine and Cu(II) ion. *Polyhedron* **2015**, *89*, 313–321. [[CrossRef](#)]
26. Kostakis, G.E.; Casella, L.; Boudalis, A.K.; Monzani, E.; Plakatouras, J.C. Structural variation from 1D chains to 3D networks: A systematic study of coordination number effect on the construction of coordination polymers using the terephthaloylbisglycinate ligand. *New J. Chem.* **2011**, *35*, 1060–1071. [[CrossRef](#)]
27. Kostakis, G.E.; Casella, L.; Hadjiliadis, N.; Monzani, E.; Kourkoumelis, N.; Plakatouras, J.C. Interpenetrated networks from a novel nanometer-sized pseudopeptidic ligand, bridging water, and transition metal ions with cds topology. *Chem. Commun.* **2005**, *987*, 3859–3861. [[CrossRef](#)] [[PubMed](#)]
28. Duan, J.; Zheng, B.; Bai, J.; Zhang, Q.; Zuo, C. Metal-dependent dimensionality in coordination polymers of a semi-rigid dicarboxylate ligand with additional amide groups: Syntheses, structures and luminescent properties. *Inorganica Chim. Acta* **2010**, *363*, 3172–3177. [[CrossRef](#)]
29. Wisser, B.; Chamayou, A.-C.; Miller, R.; Scherer, W.; Janiak, C. A chiral C₃-symmetric hexanuclear triangular-prismatic copper(ii) cluster derived from a highly modular dipeptidic *N,N'*-terephthaloyl-bis(S-aminocarboxylato) ligand. *CrystEngComm* **2008**, *10*, 461–464. [[CrossRef](#)]
30. Sun, R.; Li, Y.Z.; Bai, J.; Pan, Y. Synthesis, structure, water-induced reversible crystal-to-amorphous transformation, and luminescence properties of novel cationic spacer-filled 3D transition metal supramolecular frameworks from *N,N',N''*-tris(carboxymethyl)-1,3,5-benzenetricarboxamide. *Cryst. Growth Des.* **2007**, *7*, 890–894. [[CrossRef](#)]
31. Sun, R.; Wang, S.; Xing, H.; Bai, J.; Li, Y.; Pan, Y.; You, X. Unprecedented 4264 topological 2-D rare-earth coordination polymers from a flexible tripodal acid with additional amide groups. *Inorg. Chem.* **2007**, *46*, 8451–8453. [[CrossRef](#)] [[PubMed](#)]
32. Loukopoulos, E.; Griffiths, K.; Akién, G.; Kourkoumelis, N.; Abdul-Sada, A.; Kostakis, G. Dinuclear Lanthanide (III) Coordination Polymers in a Domino Reaction. *Inorganics* **2015**, *3*, 448–466. [[CrossRef](#)]
33. Kallitsakis, M.; Loukopoulos, E.; Abdul-Sada, A.; Tizzard, G.J.; Coles, S.J.; Kostakis, G.E.; Lykakis, I.N. A Copper-Benzotriazole-Based Coordination Polymer Catalyzes the Efficient One-Pot Synthesis of (*N'*-Substituted)-hydrazo-4-aryl-1,4-dihydropyridines from Azines. *Adv. Synth. Catal.* **2017**, *359*, 138–145. [[CrossRef](#)]
34. Loukopoulos, E.; Kallitsakis, M.; Tsoureas, N.; Abdul-Sada, A.; Chilton, N.F.; Lykakis, I.N.; Kostakis, G.E. Cu(II) Coordination Polymers as Vehicles in the A³ Coupling. *Inorg. Chem.* **2017**, *56*, 4898–4910. [[CrossRef](#)] [[PubMed](#)]
35. Kulkarni, C.; Meijer, E.W.; Palmans, A.R.A. Cooperativity Scale: A Structure–Mechanism Correlation in the Self-Assembly of Benzene-1,3,5-tricarboxamides. *Acc. Chem. Res.* **2017**, *50*, 1928–1936. [[CrossRef](#)] [[PubMed](#)]
36. Dolomanov, O.V.; Blake, A.J.; Champness, N.R.; Schröder, M. OLEX: New software for visualization and analysis of extended crystal structures. *J. Appl. Crystallogr.* **2003**, *36*, 1283–1284. [[CrossRef](#)]
37. Sheldrick, G.M. SHELXT—Integrated space-group and crystal-structure determination. *Acta Crystallogr. Sect. A Found. Adv.* **2015**, *71*, 3–8. [[CrossRef](#)] [[PubMed](#)]
38. Sheldrick, G.M. SHELXS97, Program for the Solution of Crystal Structures. *Acta Crystallogr. Sect. A* **2008**, *64*, 112–122. [[CrossRef](#)] [[PubMed](#)]
39. Sheldrick, G.M. A short history of SHELX. *Acta Crystallogr. Sect. A* **2008**, *64*, 112–122. [[CrossRef](#)] [[PubMed](#)]
40. Spek, A.L. Single-crystal structure validation with the program PLATON. *J. Appl. Crystallogr.* **2003**, *36*, 7–13. [[CrossRef](#)]
41. Farrugia, L.J. WinGX suite for small-molecule single-crystal crystallography. *J. Appl. Crystallogr.* **1999**, *32*, 837–838. [[CrossRef](#)]

42. Macrae, C.F.; Edgington, P.R.; McCabe, P.; Pidcock, E.; Shields, G.P.; Taylor, R.; Towler, M.; Van De Streek, J. Mercury: Visualization and analysis of crystal structures. *J. Appl. Crystallogr.* **2006**, *39*, 453–457. [[CrossRef](#)]
43. Stiefel, E.I.; Brown, G.F. On the Detailed Nature of the Six-Coordinate Polyhedra in Tris(bidentate ligand) Complexes. *Inorg. Chem.* **1972**, *11*, 434–436. [[CrossRef](#)]
44. Addison, A.W.; Rao, T.N.; Reedijk, J.; van Rijn, J.; Verschoor, G.C. Synthesis, structure, and spectroscopic properties of copper(II) compounds containing nitrogen-sulphur donor ligands; the crystal and molecular structure of aqua[1,7-bis(*N*-methylbenzimidazol-2'-yl)-2,6-dithiaheptane] copper(II) perchlorate. *J. Chem. Soc. Dalton. Trans.* **1984**, 1349. [[CrossRef](#)]
45. Blatov, V.A.; Shevchenko, A.P.; Proserpio, D.M. Applied Topological Analysis of Crystal Structures with the Program Package ToposPro. *Cryst. Growth Des.* **2014**, *14*, 3576–3586. [[CrossRef](#)]
46. Hao, Y.; Wu, B.; Li, S.; Jia, C.; Huang, X.; Yang, X.-J. Coordination polymers derived from a flexible bis(pyridylurea) ligand: Conformational change of the ligand and structural diversity of the complexes. *CrystEngComm* **2011**, *13*, 215–222. [[CrossRef](#)]
47. Hsu, Y.F.; Lin, C.H.; Chen, J.D.; Wang, J.C. A novel interpenetrating diamondoid network from self-assembly of *N,N'*-di(4-pyridyl)adipoamide and copper sulfate: An unusual 12-fold, [6 + 6] mode. *Cryst. Growth Des.* **2008**, *8*, 1094–1096. [[CrossRef](#)]
48. Blatov, V.A.; Carlucci, L.; Ciani, G.; Proserpio, D.M. Interpenetrating metal organic and inorganic 3D networks: A computer-aided systematic investigation. Part I. Analysis of the Cambridge structural database. *CrystEngComm* **2004**, *6*, 378. [[CrossRef](#)]
49. Allen, F.H. The Cambridge Structural Database: A quarter of a million crystal structures and rising. *Acta Crystallogr. Sect. B Struct. Sci.* **2002**, *58*, 380–388. [[CrossRef](#)]
50. Lu, Z.; Xing, H.; Sun, R.; Bai, J.; Zheng, B.; Li, Y. Water stable metal-organic framework evolutionally formed from a flexible multidentate ligand with acylamide groups for selective CO₂ adsorption. *Cryst. Growth Des.* **2012**, *12*, 1081–1084. [[CrossRef](#)]
51. Min, T.; Zheng, B.; Bai, J.; Sun, R.; Li, Y.; Zhang, Z. Topology diversity and reversible crystal-to-amorphous transformation properties of 3D cobalt coordination polymers from a series of 1D rodlike dipyriddy-containing building blocks and a flexible tripodal acid with additional amide groups. *CrystEngComm* **2010**, *12*, 70–72. [[CrossRef](#)]
52. Zuo, C.; Bai, J.; Sun, R.; Li, Y. Synthesis, structure, novel topology and reversible crystal-to-amorphous transformation of calcium coordination polymers from a flexible tripodal acid with additional amide groups. *Inorg. Chim. Acta* **2012**, *383*, 305–311. [[CrossRef](#)]
53. Karmakar, A.; Oliver, C.L.; Roy, S.; Öhrström, L. The synthesis, structure, topology and catalytic application of a novel cubane-based copper(ii) metal-organic framework derived from a flexible amido tripodal acid. *Dalton Trans.* **2015**, *44*, 10156–10165. [[CrossRef](#)] [[PubMed](#)]
54. Chen, Z.; Liu, X.; Wu, A.; Liang, Y.; Wang, X.; Liang, F. Synthesis, structure and properties of an octahedral dinuclear-based Cu 12 nanocage of trimesoyltri(L-alanine). *RSC Adv.* **2016**, *6*, 9911–9915. [[CrossRef](#)]
55. Chen, Z.; Zhang, C.; Liu, X.; Zhang, Z.; Liang, F. Synthesis, structure, and properties of a chiral zinc(II) metal-organic framework featuring linear trinuclear secondary building blocks. *Aust. J. Chem.* **2012**, *65*, 1662–1666. [[CrossRef](#)]
56. Chen, Z.; Liu, X.; Zhang, C.; Zhang, Z.; Liang, F. Structure, adsorption and magnetic properties of chiral metal-organic frameworks bearing linear trinuclear secondary building blocks. *Dalton Trans.* **2011**, *40*, 1911. [[CrossRef](#)] [[PubMed](#)]
57. Peshkov, V.A.; Pereshivko, O.P.; Van der Eycken, E.V. A walk around the A³-coupling. *Chem. Soc. Rev.* **2012**, *41*, 3790. [[CrossRef](#)] [[PubMed](#)]
58. Fan, W.; Yuan, W.; Ma, S. Unexpected E-stereoselective reductive A(3)-coupling reaction of terminal alkynes with aldehydes and amines. *Nat. Commun.* **2014**, *5*, 3884. [[CrossRef](#)] [[PubMed](#)]
59. Kaur, S.; Kumar, M.; Bhalla, V. Aggregates of perylene bisimide stabilized superparamagnetic Fe₃O₄ nanoparticles: An efficient catalyst for the preparation of propargylamines and quinolines via C–H activation. *Chem. Commun.* **2015**, *51*, 16327–16330. [[CrossRef](#)] [[PubMed](#)]
60. Paioti, P.H.S.; Abboud, K.A.; Aponick, A. Catalytic Enantioselective Synthesis of Amino Skipped Dienes. *J. Am. Chem. Soc.* **2016**, *138*, 2150–2153. [[CrossRef](#)] [[PubMed](#)]

61. De, D.; Pal, T.K.; Neogi, S.; Senthilkumar, S.; Das, D.; Gupta, S.S.; Bharadwaj, P.K. A Versatile CuII Metal-Organic Framework Exhibiting High Gas Storage Capacity with Selectivity for CO₂: Conversion of CO₂ to Cyclic Carbonate and Other Catalytic Abilities. *Chem. Eur. J.* **2016**, *22*, 3387–3396. [[CrossRef](#)] [[PubMed](#)]
62. Arcadi, A.; Cacchi, S.; Cascia, L.; Fabrizi, G.; Marinelli, F. Preparation of 2,5-disubstituted oxazoles from *N*-propargylamides. *Org. Lett.* **2001**, *3*, 2501–2504. [[CrossRef](#)] [[PubMed](#)]
63. Nilsson, B.M.; Hacksell, U. Base-Catalyzed cyclization of *N*-propargylamides to oxazoles. *J. Heterocycl. Chem.* **1989**, *26*, 269–275. [[CrossRef](#)]
64. Chauhan, D.P.; Varma, S.J.; Vijeta, A.; Banerjee, P.; Talukdar, P. A 1,3-amino group migration route to form acrylamidines. *Chem. Commun.* **2014**, *50*, 323–325. [[CrossRef](#)] [[PubMed](#)]
65. Yamamoto, Y.; Hayashi, H.; Saigoku, T.; Nishiyama, H. Domino coupling relay approach to polycyclic pyrrole-2-carboxylates. *J. Am. Chem. Soc.* **2005**, *127*, 10804–10805. [[CrossRef](#)] [[PubMed](#)]
66. Zhao, Y.; Zhou, X.; Okamura, T.-A.; Chen, M.; Lu, Y.; Sun, W.-Y.; Yu, J.-Q. Silver supramolecule catalyzed multicomponent reactions under mild conditions. *Dalton Trans.* **2012**, *41*, 5889–5896. [[CrossRef](#)] [[PubMed](#)]
67. Sun, W.J.; Xi, F.G.; Pan, W.L.; Gao, E.Q. MIL-101(Cr)-SO₃Ag: An efficient catalyst for solvent-free A³ coupling reactions. *J. Mol. Catal. A Chem.* **2016**, *430*, 36–42. [[CrossRef](#)]
68. Jayaramulu, K.; Datta, K.K.R.; Suresh, M.V.; Kumari, G.; Datta, R.; Narayana, C.; Eswaramoorthy, M.; Maji, T.K. Honeycomb porous framework of zinc(II): Effective host for palladium nanoparticles for efficient three-component (A³) coupling and selective gas storage. *Chempluschem* **2012**, *77*, 743–747. [[CrossRef](#)]
69. Lili, L.; Xin, Z.; Jinsen, G.; Chunming, X. Engineering metal–organic frameworks immobilize gold catalysts for highly efficient one-pot synthesis of propargylamines. *Green Chem.* **2012**, *14*, 1710. [[CrossRef](#)]
70. Prat, D.; Hayler, J.; Wells, A. A survey of solvent selection guides. *Green Chem.* **2014**, *16*, 4546–4551. [[CrossRef](#)]



© 2018 by the authors. Licensee MDPI, Basel, Switzerland. This article is an open access article distributed under the terms and conditions of the Creative Commons Attribution (CC BY) license (<http://creativecommons.org/licenses/by/4.0/>).